1372 *Biochemistry* **2002,** *41,* 1372−1380

Rapid Intrachain Binding of Histidine-26 and Histidine-33 to Heme in Unfolded Ferrocytochrome *c*[†]

Stephen J. Hagen,*[,‡] Ramil F. Latypov,[§] Dimitry A. Dolgikh,[||] and Heinrich Roder[§]

Physics Department, University of Florida, P.O. Box 118440, Gainesville, Florida 32611, Institute for Cancer Research, Fox Chase Cancer Center, 7701 Burholme Avenue, Philadelphia, Pennsylvania 19111, and Shemyakin-Ovchinnikov Institute for Bioorganic Chemistry, Russian Academy of Sciences, ul. Miklukho-Maklaya, 16/10, GSP-7, Moscow 117871, Russia

Received June 29, 2001; Revised Manuscript Received November 19, 2001

ABSTRACT: Time-resolved spectroscopic studies of unfolded horse iron(II) cytochrome *c* have suggested that the imidazole side chains of His26 and His33 bind transiently to the heme iron on microsecond time scales, after photodissociation of a carbon monoxide ligand from the heme. Our studies of four variants of cytochrome *c* (horse wild type, horse H33N, horse H33N/H26Q, and tuna wild type), unfolded in guanidine hydrochloride at pH 6.5, demonstrate that these side chains are responsible for the observed microsecond spectral changes. As His33 and then His26 are eliminated from the horse wild-type sequence, transient optical absorption spectra show systematic suppression of a rapid (∼10−100 μs) Soret absorbance change that follows photolysis of CO. Transient binding of these histidine side chains to the heme therefore generates one of the fast kinetic phases observed in previous photochemically triggered spectroscopic studies of dynamics in unfolded iron(II) cytochrome *c*. Furthermore, both His33 and His26 appear to contribute to a similar extent in these early kinetics. Thus, the stiffness of the polypeptide chain creates a deviation from Gaussian chain behavior by impeding, although not preventing, the formation of short (<10 peptide bonds) intrachain loops around the heme group.

Horse cytochrome *c* has been an important model system for the study of protein folding, largely owing to the properties of the heme group that is covalently attached to the polypeptide chain at positions 14 and 17. In the native structure, the side chains of His18 and Met80 bind as axial ligands to the heme iron (*1*). In the unfolded state, Met80 dissociates from the distal side of the iron while His18 remains attached to the proximal side. The 5-coordinate iron can then bind transiently to other side chains or to exogenous ligands. This property of the heme gives rise to complex dynamics prior to and during folding of the molecule, but it also makes possible a number of different methods for triggering and observing these dynamics.

The transient binding of non-native ligands at the heme, prior to folding of cytochrome *c*, has been of particular interest. Jones et al. (*2*) photodissociated a CO ligand from the reduced [i.e., Fe(II)] heme of cytochrome *c* unfolded in GdnHCl.[1] They found that this generates a sequence of rapid intrachain heme reactions on microsecond time scales. These were presumed to involve binding of the methionine residues Met65 and Met80, and the histidines His26 and His33, to the axial coordination site on the distal side of the heme iron. (The 19 lysine residues on the chain are not expected to compete for the iron coordination site at early times, since they are protonated at neutral pH.) The rates of these fast processes allow a direct estimate of the speed of intrachain contact formation in an unfolded protein, which provides insight into an important time scale in protein folding (*3*−*5*). Pascher et al. (*6*) and Telford et al. (*7*) further showed that ligand substitutions in cytochrome *c* can be investigated through laser-triggered electron injection, which reduces the unfolded Fe(III) protein to Fe(II). Recent studies that combine such techniques with transient circular dichroism and magnetic circular dichroism (MCD) have produced evidence for unusually fast folding of the cytochrome *c* molecule in GdnHCl (*8*−*10*). Those studies in fact suggest that transient heme−histidine and heme−methionine binding occur within two distinctly different, slowly interconverting, ensembles of molecules; that is, the protein exhibits kinetic heterogeneity in the unfolded state (*10*).

Interpretation of the complex intrachain dynamics of unfolded cytochrome *c* requires correct identification of the side chains that participate in these dynamics. By comparing transient Soret absorption spectra collected after nanosecond photolysis of cytochrome *c* to equilibrium spectra collected from model compounds, Jones et al. (*2*) proposed that the first kinetic phase, which is complete within 10 μs at 40 °C, corresponds to Met65 and Met80 binding at the heme. They argued that binding of His26 and His33 follows on the $\sim 10^{-4}$ s time scale. The first phase is eliminated by carboxymethylation of the methionine residues (*4*). Furthermore, it remains present at acid pH, which would not be the case if it were

---

[†] Supported by the National Science Foundation, Division of Molecular and Cellular Biosciences, Awards 0077907 (S.J.H.) and 0079148 (H.R.), and by the University of Florida, College of Liberal Arts and Sciences (S.J.H.).

* Corresponding author. E-mail: sjhagen@ufl.edu. Phone: 352-392-4716. Fax: 352-392-7709.

[‡] University of Florida.

[§] Fox Chase Cancer Center.

[||] Russian Academy of Sciences.

[1] Abbreviations: GdnHCl, guanidine hydrochloride; SVD, singular value decomposition; MCD, magnetic circular dichroism.

10.1021/bi011371a CCC: $22.00

Table 1: Histidines and Neighboring Sequence in Horse and Tuna Cytochromes *c* (Wild Type)

source of protein	residues 17-18-19	residues 25-26-27	residues 32-33-34
horse	C-H-T	K-H-K	L-H-G
tuna	C-H-T	K-H-K	L-W-G

due to His26 and His33 binding (*8*). Therefore, its assignment to Met65/Met80 binding appears well justified, although the role of His26 and His33 in these rapid intrachain binding kinetics is less firmly established.

The question of whether both His26 and His33 participate in these kinetics bears significantly on questions of conformational flexibility in unfolded polypeptides: Can very short loops form on the microsecond time scales of early folding events, and how does the stiffness of short lengths of chain generate departures from ideal Gaussian chain statistics for loop formation? His26 and His33 have been shown to play a role in the folding of oxidized [i.e., Fe(III)] cytochrome *c* from chemically denatured states, which occurs on millisecond time scales. These residues compete with Met80 for access to the heme iron (*11*, *12*) and thus create a kinetic trap that delays folding. Colón et al. (*13*) showed that the H33N mutation (His33 → Asn) eliminates a slow phase (∼8 s^{-1} at pH 5) that is observed in the refolding of the wild-type protein. By contrast, the H26Q mutation (His26 → Gln) had less effect on refolding kinetics. Thus, His33 does bind as a transient ligand in the refolding of the Fe(III) protein, while binding of His26 is slower, suggesting that steric interactions hinder the formation of the shortest intrachain loops.

However, the role of His26 and His33 in the fast kinetics that follow photodissociation of the Fe(II) protein has not been examined in detail. Chen et al. (*8*) reported that the amplitude of the second microsecond process, which Jones et al. interpreted as His26/His33 binding, is reduced in the cytochrome *c* of tuna, which lacks His33. Modeling of time-resolved MCD data also supported the assignment of this process to histidine ligation (*10*). Here we present a study of the kinetics that occur after photolysis in several histidine variants of the reduced protein. We have used nanosecond-resolved transient absorption spectroscopy to study the intrachain reaction kinetics in the wild type (WT) of cytochrome *c* from horse heart and two mutants, the single mutant H33N and the double mutant H33N/H26Q. We have also studied these kinetics in the cytochrome *c* of tuna; since the sequence for tuna resembles that of horse but lacks His33 (Table 1), we expect it to show kinetics similar to those of the horse H33N mutant. Our results demonstrate unambiguously that both His26 and His33 participate in the rapid intrachain ligand binding phenomena. We also find evidence that the two side chains bind at comparable rates to the heme iron, indicating that even short segments of the unfolded polypeptide retain the flexibility to form intrachain loops.

EXPERIMENTAL PROCEDURES

Construction and Expression of Mutant Genes and Protein Purification. WT cytochrome *c* from horse heart and from tuna were obtained from Sigma Chemical Co. and used without further purification. All of the genetic manipulations of horse cytochrome *c* were performed according to conventional protocols (*14*, *15*). The mutant genes were prepared using PCR-based mutagenesis and introduced into a plasmid pBP(*Xho*I/*Bam*HI)/3 in tandem with the gene of yeast cytochrome *c* heme lyase, *CYC3* (*16*, *17*). The sequences of mutant genes were verified by sequencing the plasmid DNA.

Cytochrome *c* mutants were produced by expression of corresponding mutant genes in JM109 (*Escherichia coli*). A single, freshly transformed colony served as the inoculum for 3−6 mL of SB media (*14*) with 1% glycerol (v/v) and 100 μg/mL ampicillin. After incubation overnight at 37 °C with vigorous shaking (250−300 rpm, New Brunswick 655D platform shaker), 0.5−1 mL was used to inoculate 1 L of SB (1% glycerol, 100 μg/mL ampicillin) in a 2.8 L flask (Pyrex, No. 4420). This culture was incubated with good aeration for 21−24 h before the cells were harvested by centrifugation (Sorvall GS-3 rotor, 4000 rpm, 15 min, 4 °C). The cell pellet was resuspended in 50 mM sodium phosphate buffer, pH 7.0. The suspension was passed twice through a precooled French press (1200 psi) and centrifuged to remove cell debris (Sorvall SA-600 rotor, 15000 rpm, 20−30 min, 4 °C). Pink supernatant was saturated stepwise first up to 55% of ammonium sulfate saturation and centrifuged (Sorvall SA-600 rotor, 15000 rpm, 20−30 min, 4 °C) and then up to 95% and centrifuged again. The final supernatant was dialyzed against several changes of 50 mM sodium phosphate buffer, pH 7.0, in 3500 MWCO dialysis tubing (Spectra/Por, Spectrum). Prior to column fractionation, cytochrome *c* was oxidized by potassium ferricyanide (1−5 mM final concentration). Then the solution was applied on a Bio-Rex 70 cation-exchange column (Bio-Rad) equilibrated with 50 mM sodium phosphate, pH 7.0. After extensive wash of the column with the same buffer (6−8 column volumes), the protein was eluted with a linear NaCl gradient around 0.25 M, and a brown fraction of oxidized cytochrome *c* was collected. Fractions with an *R*-value (A_{409}/A_{280}) between 4.5 and 5.0 were pooled and dialyzed against 50 mM ammonium bicarbonate buffer (pH 7−8) prior to lyophilization. The purity of the protein was examined by gel electrophoresis in 16.5% Tris-Tricine Ready Gel (Bio-Rad), and the protein redox state was confirmed by measuring absorbance in the 500−600 nm region (absence of sharp bands at 520 and 550 nm) or by calculating a ratio A_{530}/A_{550} which should be around 1.3−1.4 for oxidized cytochrome *c*. Intactness and identity of the mutant proteins were confirmed by MALDI mass spectrometry (Voyager-DE, PerSeptive Biosystems). The protein concentration was determined spectrophotometrically on the basis of an extinction coefficient of 1.06 × 10^5 (M cm)$^{-1}$ at 409 nm for oxidized cytochrome *c* (*18*).

Transient Spectroscopy. We used a nanosecond laser pulse to photodissociate a carbon monoxide ligand from the heme iron of the cytochrome *c* in the Fe(II) form, unfolded in GdnHCl. We then collected the transient absorption spectra in the heme Soret region, where spectral changes indicate the changes in the heme iron coordination. All proteins were dissolved in 5.00 M GdnHCl and 100 mM phosphate buffer, pH 6.5 at 22 °C. GdnHCl concentrations were measured refractometrically. Samples were passed through an 0.2 μm syringe filter and then deoxygenated under flowing CO for 30 min at room temperature. After trace sodium dithionite was added to reduce the heme iron to the Fe(II) state, samples were sealed in quartz cuvettes (0.5 mm path length) and equilibrated overnight. Protein concentrations were 70−100 μM.

The transient absorption spectrometer has been described previously (*5*). Briefly, 5−7 ns pulses generated by a frequency-doubled Nd:YAG laser, at 532 nm and a repetition rate of up to 10 Hz, are focused onto the sample cuvette to an energy density ∼4 mJ/mm^2, photodissociating the CO from the heme iron. At a delay time t after each laser pulse, a flash from a short-arc Xe flashlamp generates sample and reference beams of white light that probe the sample absorbance in the range 390−450 nm. The CO eventually rebinds to the heme, and the protein recovers completely (at t ∼0.1−1 s). The photolysis and probe beam paths intersect at an angle of 38°, and delay times can be adjusted from less than 10 ns to milliseconds or many seconds as needed. Nanosecond-resolved spectra are obtained by dispersing transmitted light in an 0.3 m spectrograph and onto a gated, intensified charge-coupled device. Transient absorbance spectra were collected at $T = 18-46$ °C, with each data set covering 75 delay time values spaced logarithmically from 10 ns to (typically) 350 ms. The temperatures of both the quartz cuvette and its immediate environment were monitored with ultraminiature chromel/alumel thermocouples during absorbance measurements; these temperatures were equal and stable to within ±0.2 °C.

Data Analysis and Fitting. The transient spectra were analyzed to give the difference optical extinction relative to the equlibrium state, i.e., $\delta\epsilon(\lambda,t) = \epsilon(\lambda,t) - \epsilon(\lambda,\infty)$, for each set of experimental conditions (i.e., each protein and temperature). We used singular value decomposition (SVD) both to provide insight into their spectral and kinetic content and to reduce the size of the data sets in order to improve the computational efficiency of data fitting. The application of SVD to absorbance spectroscopic data has been reviewed elsewhere (*19*). SVD decomposes the matrix of transient absorbance measurements, $\delta\epsilon\ (\lambda,t)$, into a product of three matrices, $\delta\epsilon(\lambda,t) = \mathbf{u}(\lambda)\mathbf{s}\mathbf{v}(t)^{\mathrm{T}}$, where the columns of the matrix $\mathbf{u}(\lambda)$ form a set of orthonormal basis spectra for the data set, and the columns of $\mathbf{v}(t)$ are orthonormal time courses associated with the basis spectra. $\mathbf{s}$ is a diagonal matrix whose elements (i.e., the singular values) are weighting factors, ordered from largest to smallest (i.e., $s_1 > s_2 > s_3$ etc.), so that the first n SVD components (i.e., the first n singular values and their associated time courses and spectra) provide the best n component description of the complete data set.

To extract information about the reaction rates that underly the spectroscopic changes following photodissociation of CO from unfolded cytochrome *c*, we fit the time-resolved absorbance spectra to a model of multiple exponential decays. More specifically, we used a Nelder−Mead simplex method to fit the five leading columns of $\mathbf{v}(t)\mathbf{s}$ from each data set simultaneously to a sum of exponential decays. The decay rates are specified by the fitting parameters (see below) while the associated wavelength-dependent decay amplitudes (for any given set of rates) are derived from the **vs** data and the exponential decay functions together through matrix division. This method combines information from the full range of wavelengths (390−440 nm) and delay times (10 ns to 350 ms) studied, with equal weighting, and is equivalent to a global analysis. It is, however, far more efficient computationally (*19*). Uncertainties in the fit parameters were estimated in a bootstrap Monte Carlo analysis.

At least four separate decay rates are required to provide a satisfactory fit to most of the data sets over the complete time range (10 ns ≤ t ≤ 350 ms). However, even a multiwavelength analysis cannot guarantee that fitting time-resolved absorbance data to multiple exponentials will generate consistent and stable results. The rates obtained may vary according to the range of experimental times and wavelengths that are analyzed; inconsistent results may also be obtained for data collected under different conditions as the underlying spectra shift with sample and temperature. This ambiguity reflects the mathematical reality that the extraction of a sum of exponential decays from a noisy signal is an ill-conditioned problem in general. The number of exponential components in the data and their associated decay rates are sensitive to noise and are not determined uniquely by the data. Multiwavelength fits may improve the situation (*20*) but do not resolve it entirely if the data arise (as ours do) from a set of generally similar heme Soret spectra.

To obtain consistent results, we found it necessary to impose constraints on the relaxation rates. One approach was simply to fit a minimal number of exponentials (i.e., 3 or 4) to each data set; this approach did not, however, cleanly resolve the histidine-mutation-sensitive processes from other processes in the data. An alternative approach was to assume a chemical kinetic model for intrachain ligand binding in cytochrome *c*, in which most of the fit parameters, i.e., the rates, are required to be independent of histidine mutations; only rates related to His26 and His33 binding were allowed to vary between mutants. For each experimental temperature, the fitting routine starts with a set of trial values for the underlying rates in the kinetic model, modifies that model by removing the His33 or His26/His33 interactions as appropriate for each mutant, calculates the anticipated relaxation rates for each mutant within the model, and then tests those rates for their suitability as exponential decay rates of the absorbance data $\mathbf{v}(t)\mathbf{s}$. In this way all four samples, and all times and wavelengths, are fit simultaneously at each temperature. Given a set of model rates and the absorbance data from each mutant, the fitting routine obtains the relaxation rates by calculating the eigenvalues of the rate matrix of the chemical model (as modified for that mutant). The model is summarized by Scheme 1.

This analysis considers only kinetics,and does not attempt to model or interpret the actual spectroscopic changes: complete modeling of transient spectra requires a detailed model for the spectra of all relevant underlying species (*2*, *5*). A disadvantage of this method is that the fit introduces 10 rate parameters, even though some of these are underdetermined. (Scheme 1 employs more kinetic rates than there are exponential relaxations in the data.) However, the eigenvalues of the rate matrix, which correspond to the observable relaxation rates, are well determined by the fit.

RESULTS

Since the spectroscopic data are complex and multiphasic in general, we consider first a simple and model-independent view of the results. Figure 1 shows $\delta\epsilon(\lambda,t) = \epsilon(\lambda,t) - \epsilon(\lambda,10\ \mathrm{ns})$, or the early changes in optical extinction, relative to the photoproduct that is present immediately after the laser pulse photolyzes the CO−iron bond in the unfolded cyto-

Scheme 1: Kinetic Model for Transient Heme Ligation Events Following Photodissociation of CO from Unfolded Horse Cytochrome *c*[a]

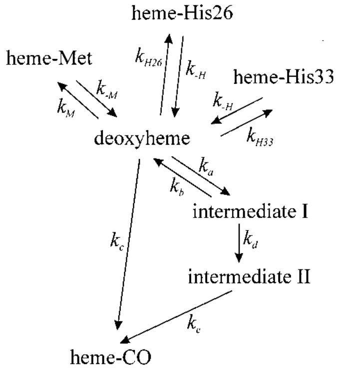

[a] The rate matrix of the model yields a set of eigenvalues (decay rates) that were used to fit the heme absorbance data as a sum of exponential decays. In modeling the tuna WT and horse H33N data, we omit the His33 state from the model; in modeling the H33N/H26Q data, we omit both the His33 and His26 states. For each temperature, the rates in this scheme were varied in order that the eigenvalues of the rate matrix provided the best possible multiexponential fit to all of the cytochrome *c* absorbance data.

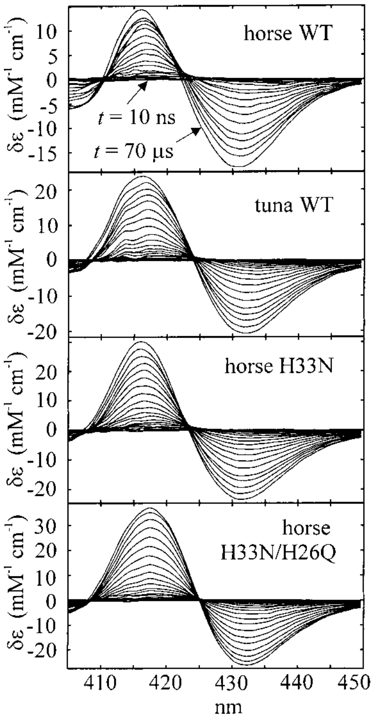

FIGURE 1: Transient change in optical extinction, $\delta\epsilon(\lambda,t) = \epsilon(\lambda,t) - \epsilon(\lambda,10\ \text{ns})$ (i.e., change relative to 10 ns photoproduct), observed in iron(II) cytochrome *c* at submillisecond times (10 ns $\le t \le$ 70 μs) after photodissociation of CO from the heme iron by a laser pulse at $t = 0$. All samples are in 5.00 M GdnHCl and 0.1 M phosphate, pH 6.5 at $T = 22$ °C. Experimental times are 10, 22, 40, 67, 100, 150, 230, 340, 510, and 760 ns and 1.1, 1.6, 2.3, 3.4, 5.0, 7.5, 11, 16, 23, 33, 48, and 70 μs.

chrome *c*. The initial spectrum evolves within a few microseconds, with increasing absorbance near 417 nm and decreasing absorbance near 432 nm. This early spectral change reflects the rapid binding of the sulfur of Met80 or Met65 to the deoxyheme, creating a subpopulation of intrachain-liganded molecules (*4*).

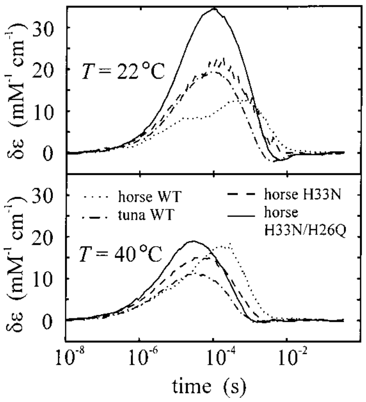

FIGURE 2: Transient changes in extinction coefficient, $\delta\epsilon(\lambda,t) = \epsilon(\lambda,t) - \epsilon(\lambda,10\ \text{ns})$ observed at fixed wavelength in the four cytochrome *c* samples. Solution conditions are as in Figure 1. (Upper panel) Data at the deoxyheme/carbonmonoxyheme isosbestic point, $\lambda = 419.5$ nm, at $T = 22$ °C. (Lower panel) Data at $T = 40$ °C, $\lambda = 419.6$ nm.

Figure 1 shows that, although the isosbestic point of the deoxyheme and heme−methionine spectra is near 425 nm, the spectral changes in the horse WT protein do not show a clear isosbestic point near this wavelength. At least one additional kinetic process evidently coincides temporally with methionine binding. By contrast, $\delta\epsilon(\lambda,t)$ for the horse double mutant H33N/H26Q very clearly shows the isosbestic point on this time scale. The figure also shows the transient spectra in samples where His33 is absent but His26 remains (i.e., the tuna WT and the horse H33N); these do not precisely match either the horse WT or the double mutant. They are instead consistent with a reduced amplitude of the additional kinetic phase. The data in Figure 1 therefore imply that the binding of the imidazole side chains of His26 and His33 at the heme gives rise to a rapid kinetic process after photolysis of CO and that both residues participate in this process.

Figure 2 shows transient extinction changes versus time, at fixed wavelength. Since the rebinding of CO to deoxyheme dominates $\delta\epsilon(\lambda,t)$ at most wavelengths and obscures the small spectral changes associated with intrachain ligand binding, the figure shows the optical density near the isosbestic point of the deoxyheme and carbonmonoxyheme spectra, $\lambda \approx$ 419.5 nm. Since this is near the peak of the methionine−heme absorbance (~417 nm), the initially rising absorbance seen in all samples indicates Met65 and Met80 binding to the deoxyheme. The single histidine variants (tuna WT and H33N) exhibit closely similar kinetics that clearly differ from those of both the horse WT and the double mutant H33N/H26Q, especially on the time scale $t \sim 10-100$ μs. At 22 °C, removal of His33 and then His26 systematically simplifies the fast kinetics, demonstrating that both residues play a comparable role in the early time kinetics.

Figure 2 also suggests that the histidine side chains compete, at least to some extent, with Met65/Met80 for access to the deoxyheme. Removing His26 and His33 increases the total absorbance change during the Met65/Met80 binding phase at $T = 22$ °C, at $\lambda = 419.5$ nm. At this temperature and wavelength, the absorbance of the methionine complex of Fe(II)−heme exceeds that of the imidazole complex by ~20−25 (mM cm)$^{-1}$ (*7*), so if removing the histidine residues tends to replace the histidine complex with the methionine complex, one expects the observed increase in total absorbance. The full absorption spectra observed at ~50 μs (Figure 3) also indicate that the total amplitude of the early spectral change is larger in the

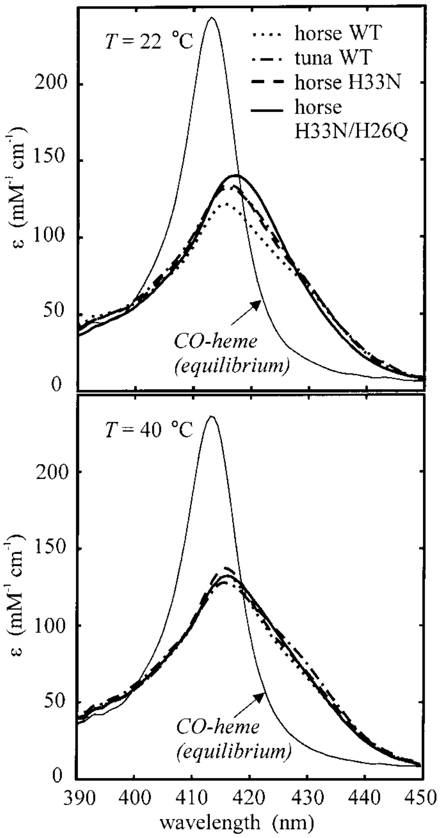

FIGURE 3: Transient optical absorption spectra collected 50 μs after photodissociation of CO, at $T = 22$ °C (upper) and 40 °C (lower). The equilibrium (carbonmonoxyheme) spectrum is also shown. Solution conditions are the same as in Figure 1.

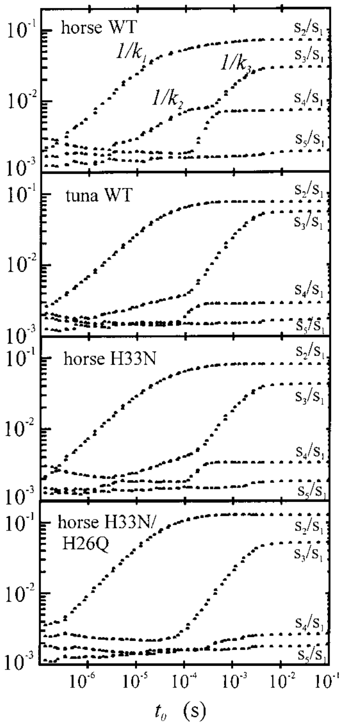

FIGURE 4: Magnitude of singular values obtained by SVD of transient absorption difference spectra, $\delta\epsilon(\lambda,t)$, as a function of the final time point included in the SVD analysis. The difference optical density data set is truncated to include only data at $t \leq t_0$, and then decomposed by SVD. The figure shows the (relative) size of the largest singular values in the SVD, as a function of t_0. Samples are in 5.00 M GdnHCl and 0.1 M phosphate, pH 6.5 at $T = 18$ °C. See Appendix.

histidine mutants. The data at 40 °C are less transparent, most likely because the imidazole and methionine complexes have very similar absorbance at this temperature (*4*); the observed amplitudes are too similar to allow a detailed comparison.

DISCUSSION

Components by SVD Analysis. Several kinetic phases appear in transient absorption spectra collected after the photodissociation of CO from unfolded iron(II) cytochrome *c*. Results of previous spectroscopic studies have been consistent with transient binding of histidine side chains as the origin of one early phase in these kinetics (*2*, *8*, *10*). Figures 1 and 2 support this picture; eliminating first His33 and then His26 from horse cytochrome *c* systematically alters the initial kinetics observed in transient absorption. An SVD analysis demonstrates more directly that binding of His26 and His33 to the heme generates one of the kinetic phases that follow photodissociation of CO.

The singular values s_1, s_2, s_3, etc. obtained through SVD of an absorption data set $\delta\epsilon(\lambda,t)$ indicate the relative importance of the independent spectral components in the data set (*19*). Thus, the number of singular values (that exceed a noise background) represents an upper limit to the number of species present that can be distinguished spectroscopically. Since we measure transient difference spectra, $\delta\epsilon(\lambda,t) = \epsilon(\lambda,t) - \epsilon(\lambda,\infty)$, the number of detectable species is one greater than the number of significant singular values. Truncating a data set $\delta\epsilon(\lambda,t)$ to exclude points collected at $t > t_0$, and then decomposing that subset of the data by SVD, reveals the number of species that are resolvable in the sample at time t_0.

Figure 4 shows how additional singular values rise above the background [which is at roughly $(1-2) \times 10^{-3}$] in the data as t_0 increases, indicating new spectral components that become detectable at longer times. The rising portions of the curves reflect the growing concentration of new transient species; the amplitude of the curves is governed by both the peak concentrations and the character of the associated spectral changes, including the degree to which they differ from spectra already present in the data (see Appendix). Four spectral components (i.e., s_1-s_4) are clearly significant in the horse WT data. The figure shows that, at $T = 18$ °C, three of these appear on time scales of roughly $1/k_1 \sim 10$ μs, $1/k_2 \sim 100$ μs, and $1/k_3 \sim 1$ ms, respectively. The fourth process is not apparent in Figure 4, since it is primarily described by the time course of the first SVD component (characterized by s_1); Figure 4 shows the size of the other singular values s_i ($i = 2-5$) relative to s_1. Previous work (*4*, *10*) attributes the initial kinetic phase, k_1, to transient binding of Met65/Met80 at the heme. The k_2 phase appears in the WT horse data and also, with very similar rate but half the amplitude, in the horse H33N and tuna data. It vanishes entirely in the H33N/H26Q mutant. Figure 4 therefore identifies the k_2 phase as a spectroscopic signature of the transient binding of both His26 and His33 to the heme iron on the ~100 μs time scale. Data at higher temperatures are similar.

The third (k_3) and fourth (k_4) kinetic phases in the data occur on millisecond time scales of roughly 0.1–1 ms and 1–10 ms, respectively (with rates increasing as T increases from 18 to 46 °C). These phases are associated with CO rebinding: Chen et al. also observed these kinetic phases, with rates of 225 μs^{-1} and 880 μs^{-1} at 40 °C, in photolysis studies of unfolded CO-cytochrome *c*, and found their rates to vary in proportion to CO partial pressure (*8*). Finding that the faster of these processes exhibits no signature in time-resolved near-UV circular dichroism, those authors proposed that the two phases may correspond to CO recombination to molecules of different tertiary structure, such as unfolded versus compact or partially folded. An alternative explanation is proposed by Arcovito et al. (*21*), who find that two CO-sensitive phases also appear after photodissociation of CO from several other forms of heme, including unfolded horse cytochrome *c*, the heme undecapeptide (microperoxidase), and free heme plus imidazole. Those authors note that photolysis of CO is likely to cause dissociation of the proximal His18, leading to formation of a 4-coordinate iron state (*22*). Since the 4-coordinate iron reacts more rapidly with CO than does the 5-coordinate iron, Arcovito et al. suggest that the 4-coordinate species rebinds CO after photolysis, leading to formation of another intermediate, possibly a 6-coordinate H_2O–Fe–CO species, which later decays to the equilibrium His18–Fe–CO. Thus they argue that the more rapid CO-sensitive phase observed in cytochrome *c* photolysis studies corresponds to rebinding of CO to 4-coordinate iron, which generates the H_2O-liganded species, while the slower CO-sensitive phase represents the replacement of the H_2O ligand by the native His18 ligand.

Kinetic Model for Rates. It is tempting to seek information about binding rates by decomposing each data set into a sum of exponential decays. At least four exponentials are required to generate a satisfactory fit to the data at all measured wavelengths and times; however, this decomposition is not unique, and it requires some constraints in order to generate decay rates that are reasonably robust with respect to changes in the wavelength or time range analyzed or to condition-dependent changes in the underlying spectra, etc. We obtained a stable and consistent set of decay rates from the absorbance data by assuming a chemical kinetic model for the heme ligation reactions in cytochrome *c* and then seeking values of the underlying rates in that model such that the overall eigenvalues of the model matched the relaxation rates observed in the data.

The model (see Scheme 1) incorporates the essential ingredients of (1) transient binding of methionine residues, (2) transient binding of His26 and/or His33, and (3) two pathways for rebinding of CO. Two intermediate states are postulated in order to generate the observed number (≥4) of exponential processes in the absorbance data of all samples (including the H33N/H26Q double mutant) and also to generate the observed two CO rebinding pathways. The intermediates may arise from base elimination (*21*), partial folding (*8*), or some other mechanism. For simplicity the binding of Met65 and Met80 is represented as a single process at a rate k_M (i.e., $k_M \cong k_{M65} + k_{M80}$); this eliminates one parameter from the model, with little effect on the results. The interactions of Met65 and Met80 with the heme have been analyzed in detail elsewhere (*5*). The eigenvalues of the rate matrix associated with Scheme 1 should then determine the relaxation rates for each mutant of cytochrome *c*, with the His33 and/or His26/His33 interactions removed from the model as appropriate, depending on the mutant. This constitutes a constraint that, for all of the studied variants of cytochrome *c*, the relaxation rates of the absorbance data are eigenvalues of a kinetic system derived from the same set of fundamental rates. This analysis does not model or interpret the actual spectral changes associated with these decays.

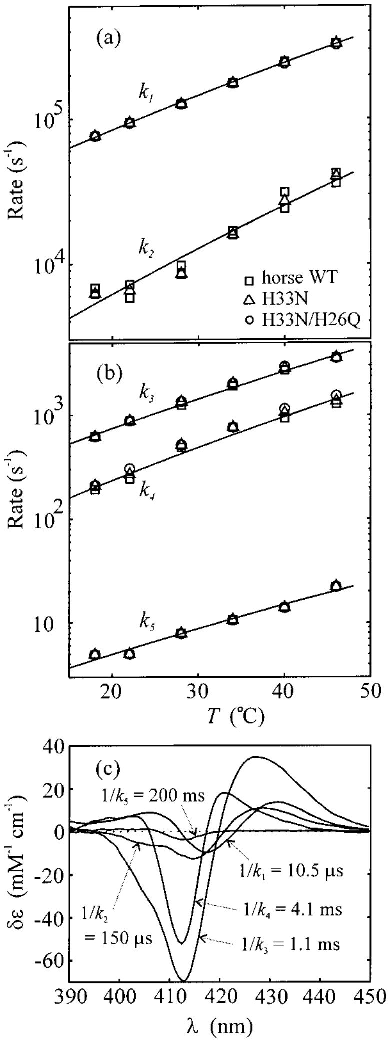

FIGURE 5: Decay rates (a) k_1 and k_2 and (b) k_3–k_5 obtained in a multiexponential fit (covering all wavelengths) to the $\delta\epsilon(\lambda,t)$ data from the cytochrome *c* variants, based on Scheme 1 (see text). Two sets of k_2 values are shown for the horse WT, since the two histidine residues give rise to a pair of similar eigenvalues at each temperature. Arrhenius fits to the horse WT rates are shown. (c) Transient spectra associated with a multiexponential fit to the horse WT data at 22 °C. For example, the most rapid process, k_1, observed in the horse WT is associated with a curve, $P(\lambda)$, in panel c; it corresponds to a time-dependent spectral change, $P(\lambda)\exp(-k_1t)$, in the horse WT $\delta\epsilon(\lambda,t)$ data set. The $P(\lambda)$ are obtained by a matrix division of the horse WT absorbance data by the exponential decay functions.

Figure 5 shows the decay rates obtained. These values provide an excellent fit to the data and agree well with rates previously reported for the horse WT (*5*, *8*). Table 2 gives the Arrhenius parameters for these rates. Aside from the complete disappearance of one kinetic process in the double mutant, Figure 5 shows that the mutations otherwise have little effect on the decay rates: the removal of H33N by

Table 2: Relaxation Rates Obtained in a Multiexponential Fit to Absorbance Data for Wild-Type Cytochrome *c*, Together with Parameters from an Arrhenius Fit to the Rates, $k = A_0(T/T_0) \exp(-E_a/k_BT)$, with $T_0 = 295$ K[a]

	value at 22 °C (s^{-1})	E_a (kJ/mol)	log A_0 (s^{-1})
k_1	$(9.5 \pm 0.6) \times 10^4$	40.6 ± 1.4	12.2 ± 0.2
k_2	$(6.2 \pm 0.9) \times 10^3$	54 ± 3	13.3 ± 0.5
k_3	$(8.8 \pm 0.5) \times 10^2$	48.4 ± 1.6	11.5 ± 0.3
k_4	$(2.4 \pm 0.4) \times 10^2$	54 ± 2	12.0 ± 0.4
k_5	5.0 ± 0.6	42 ± 5	8.2 ± 0.9

[a] The parameters for the histidine mutants are not significantly different, although k_2 is absent in the H33N/H26Q mutant (see text).

mutation does not affect the rate of the k_2 process. This result is a simple consequence of Scheme 1. Analysis of the fit results shows that the faster time constants in the experimental data (i.e., faster than $\sim 10^3$/s at 22 °C) are determined by the deoxyheme−histidine−methionine subsystem alone (involving k_M, k_{-M}, k_{H26}, k_{H33}, and k_{-H}), in which most of the rates exceed 10^4/s. The rate matrix of the subsystem describing histidine and methionine binding has three nonzero eigenvalues, which can be obtained analytically: one eigenvalue is precisely k_{-H}, the second is very nearly k_{-H}, and the third is approximately $k_M + k_{-M}$, or the equilibration rate of heme−methionine reaction. Thus the wild type and the single His33 mutants exhibit one fast relaxation (k_1) that primarily reflects methionine binding and one or two slower relaxations at a rate k_{-H}, resulting from transient binding of His26 or His33. The single mutations H33N or H33W do not significantly change these rates, although of course the double mutation H33N/H26Q eliminates the k_{-H} rate.

The slower time constants in the data (k_3−k_5 in Figure 5) are controlled by k_a−k_e of Scheme 1, all of which are evidently slow, at least 10-fold slower than k_{-H}. For example, the observed relaxation rates at 22 °C are consistent with $k_a \sim 18\ s^{-1}$, $k_b \sim 0.6\ s^{-1}$, $k_c \sim 0.6\ s^{-1}$, $k_d \sim 300\ s^{-1}$, and $k_e \sim 5\ s^{-1}$, although the actual values of these parameters are not well determined by the kinetic fit.

Estimation of Rates. Although the exponential decay rates in the data are well determined in the kinetic analysis, extracting the underlying rates of Scheme 1 would require a detailed modeling of the spectral changes and amplitudes. This in turn requires better understanding of the subsequent phases and intermediates associated with CO rebinding. Nevertheless, since the heme−histidine dissociation rate k_{-H} is an eigenvalue of the heme−histidine−methionine subsystem, we obtain a fairly confident estimate, $k_{-H} \approx (5.8 \pm 0.7) \times 10^3\ s^{-1}$ at 22 °C and $k_{-H} \approx (2.4 \pm 0.3) \times 10^4\ s^{-1}$ at 40 °C. These rates closely match the dissociation rate measured for the bimolecular heme−histidine complex, $k_d \approx (7.2 \pm 0.8) \times 10^3\ s^{-1}$ at 22 °C and $(2.6 \pm 0.6) \times 10^4\ s^{-1}$ at 40 °C (*4*) under these solution conditions. This agreement demonstrates that heme−histidine binding is reaction controlled. Therefore, the binding rates k_{H33} and k_{H26} in Scheme 1 are $k_{H26} \approx P(8)k_g$ and $k_{H33} \approx P(15)k_g$, where $P(8)$ and $P(15)$ are the equilibrium probabilities for the formation of the ∼8 and ∼15 residue intrachain loops that bring His26 and His33 into proximity with the heme and k_g is the deoxyheme−histidine geminate reaction rate [$k_g \approx 6 \times 10^7\ s^{-1}$ at 22 °C, pH 6.5 (*4*)]. Equivalently, we can write $k_{H26} \sim C_{H26}k_{bi}$ and $k_{H33} \sim C_{H33}k_{bi}$, where C_{H26} and C_{H33} are the effective concentrations of His26 and His33 at the heme iron in the unfolded protein and $k_{bi} \sim (2.7 \pm 0.2) \times 10^5\ M^{-1}\ s^{-1}$ is the bimolecular rate for histidine binding to ferrous heme (*4*).

The kinetics alone do not shed much light on k_{H33} and k_{H26} since, unless these rates are both close to k_{-H}, they do not greatly affect the eigenvalues of Scheme 1. Our fit indicates $k_{H33} + k_{H26} \sim (2 \pm 1) \times 10^3\ s^{-1}$ for $T \sim 20$−30 °C, but the ratio k_{H33}/k_{H26} is not well determined. However, the spectroscopic data in Figures 1 and 2, and especially Figure 4, suggest the simple interpretation that removing His33 reduces the amplitude of the histidine binding phase by almost exactly 50%. This implies that k_{H26} and k_{H33} are nearly equal, or $k_{H26} \approx k_{H33} \approx (1 \pm 0.5) \times 10^3\ s^{-1}$ near 20 °C, giving an equilibrium constant $k_{H26}/k_{-H} \sim 0.2$. Thus $P(8) \approx P(15) \approx (1.7 \pm 0.8) \times 10^{-5}$, or $C_{H26} \approx C_{H33} \approx (3.7 \pm 1.8)$ mM.

This effective concentration is consistent with equilibrium NMR studies, which indicated that the effective concentration of nearby histidine side chains at the heme of unfolded cytochrome *c* is in the range of 3−8 mM (although possibly as large as 16 mM) in 3.5 M GdnHCl (*23*). However, the evidence that k_{H26} and k_{H33} are roughly equal, and therefore that $P(8) \approx P(15)$, indicates that the unfolded polypeptide departs significantly from the behavior expected for an ideal polymer chain that is assumed in ref *23*. For the ideal chain, the probability of forming an intrachain loop of *n* residues is proportional to $n^{-3/2}$ (*24*), or $P(8) \approx 2.5\ P(15)$. The finite stiffness of short segments of a real polypeptide must generate a departure from ideal behavior as *n* becomes quite small. Camacho and Thirumalai (*25*, *26*) have estimated $P(n)$ for the formation of disulfide linkages in short polypeptides and predict that loops of $n \approx 10$ residues form with the highest probability, while $P(n)$ drops sharply for shorter loops. They calculate relative probabilities of 0.3:0.7:1.0:0.5 for intrachain loops of 8, 9, 10, and 15 residues, respectively. Given the uncertainty in defining the contour length of the His26 loop as 8 residues, the starting point could be considered as His18 or as another point between Cys14 and Cys17, the probability for intrachain loop formation in unfolded cytochrome *c* does appear consistent with the model of Camacho and Thirumalai; the data suggest $P(8) \approx P(15)$, indicating that the anticipated "roll-off" of the loop formation probability does occur near $n \sim 10$. Studies of loop formation kinetics in flexible synthetic peptides have also suggested (although not directly observed) a roll-off at $n \sim 10$ (*27*, *28*).

Finally, we consider briefly the question of whether a homogeneous or inhomogeneous model better describes the loop formation dynamics that occur after photolysis. Goldbeck et al. (*10*) recently reported that modeling of transient MCD spectra in guanidine-unfolded iron(II) cytochrome *c* strongly favors an inhomogeneous model, in which two to three slowly interconverting subpopulations of molecules coexist in the unfolded state. That is, ∼20% of unfolded cytochrome *c* molecules are in a conformation that allows transient binding of methionine within microseconds of photolysis, while a separate population (∼60%) can transiently bind histidine; the two ligation processes are then kinetically uncoupled, at least on time scales ≤100 μs. On the basis of the rapid appearance of about 10% of the nativelike far-UV circular dichroism, these authors argued that the methionine binding ensemble in fact proceeds to the folded state in ∼1 μs (at 40 °C), while the histidine binding ensemble remains kinetically trapped. In our data, however, the overall amplitude of the rapid spectral changes observed in the histidine variants, and compared to the horse WT (Figures 2 and 3), does not suggest that eliminating the histidine side chains reduces the total fraction of hemes that bind ligands in the initial ∼100 μs after photolysis. At $T =$ 22 °C the mutations actually seem to increase the total amplitude of the Met65/Met80 binding. This finding supports a homogeneous model for the intrachain ligand binding kinetics (*2*), in which the His26/His33 side chains compete with the Met65/Met80 side chains for access to the deoxyheme after photolysis of CO. In this case, the rapid CD changes observed by Chen et al. (*8*) may indicate partial formation of secondary structure in a large number of molecules, rather than complete folding of a small fraction.

ACKNOWLEDGMENT

The authors thank Erik Sjolander for composing LabView software, Linlin Qiu for providing assistance with Maple, and Andrea Bellelli for helpful discussions of base elimination in heme proteins.

APPENDIX

Interpretation of Figure 4. Figure 4 shows how several new, spectroscopically distinguishable species appear in the absorbance data sets on various time scales. Some additional discussion of singular value decomposition (SVD) may help in understanding this figure. If the matrix $\mathbf{A} = \mathbf{A}(\lambda,t)$ contains the time- and wavelength-resolved absorbance data obtained in a spectroscopic measurement under given experimental conditions (i.e., one sample at one temperature T), then the SVD of $\mathbf{A}$ is given by $\mathbf{A} = \mathbf{USV}^\mathrm{T}$. Here the columns of $\mathbf{U}$ are a set of orthonormal basis spectra, $U_i(\lambda)$, and the columns of $\mathbf{V}$ are orthonormal functions of time, $V_i(t)$. The singular values s_i are elements of the diagonal matrix $\mathbf{S}$ and are nonnegative. Furthermore, the columns of $\mathbf{V}$ are the eigenvectors, and the elements of $\mathbf{S}^2 = \mathbf{S}^\mathrm{T}\mathbf{S}$ (a diagonal matrix) are the eigenvalues, of the matrix $\mathbf{A}^\mathrm{T}\mathbf{A}$. Similarly, the columns of $\mathbf{U}$ are the eigenvectors, and the elements of $\mathbf{S}^2$ are the eigenvalues, of the matrix $\mathbf{AA}^\mathrm{T}$.

Formally, the number of nonzero singular values gives the rank of $\mathbf{A}$. In a real data set, the number of singular values that exceed some floor value (determined by experimental noise) indicates an effective rank for $\mathbf{A}$, or the number of spectroscopically distinguishable species in the data. (The total number of species present may be larger.) How is the SVD of a data set affected by the appearance of a new chemical species? We consider a spectroscopic data set $\mathbf{A}_0(\lambda,t)$ that becomes perturbed by the appearance of a new chemical species. The perturbation $\epsilon(\lambda,t)$ added to $\mathbf{A}_0(\lambda,t)$ normally contains spectral components that are linear combinations of existing spectral components in $\mathbf{A}_0$, as well as components that are orthogonal to the spectra comprising $\mathbf{A}_0$. Here we are interested in a perturbation that generates "new" spectral content in the data, i.e., one that is described by a previously unimportant basis spectrum $U_i(\lambda)$ and therefore causes the singular value s_i to increase above its original background level s_i^o. Perturbations that can be represented as linear combinations of existing spectral components do not generate new singular values. Given a small change in the data set $\mathbf{A}_0$

$$\mathbf{A} = \mathbf{A}_0 + \epsilon$$

perturbation theory describes the effect of ϵ on the singular values of $\mathbf{A}$, or (equivalently) the eigenvalues of $\mathbf{AA}^\mathrm{T} = \mathbf{A}_0\mathbf{A}_0^\mathrm{T} + \mathbf{W}$, where $\mathbf{W} = \mathbf{A}_0\epsilon^\mathrm{T} + \epsilon\mathbf{A}_0^\mathrm{T} + \epsilon\epsilon^\mathrm{T}$. The unperturbed singular value s_i^o is shifted according to

$$s_i^2 = s_i^{\mathrm{o}2} + U_i^\mathrm{T}\mathbf{W}U_i + \sum_{j\neq i}(U_i^\mathrm{T}\mathbf{W}U_j)^2/(s_i^{\mathrm{o}2} - s_j^{\mathrm{o}2}) + ... \tag{A1}$$

(*19*). Once the term $U_i^\mathrm{T}\mathbf{W}U_i$ exceeds the "background" value of $s_i^{\mathrm{o}2}$, s_i^2 grows linearly with $U_i^\mathrm{T}\mathbf{W}U_i$. Consistent with the idea of a new spectral component appearing in a chemical kinetic relaxation of rate k, we consider the situation

$$\epsilon(\lambda,t) = \epsilon_i U_i(\lambda)R(t)$$

where ϵ_i is a constant, $U_i(\lambda)$ is a column vector (a normalized basis spectrum), and $R(t)$ is a row vector with elements $R_j = 1 - \exp(-kt_j)$, and $\{t_j\}$ is the set of experimental time delays. Since the basis spectrum $U_i(\lambda)$ associated with ϵ is orthogonal to those that comprise $\mathbf{A}_0$, one may show that the terms in $\mathbf{W}$ that are linear in ϵ do not contribute to $U_i^\mathrm{T}\mathbf{W}U_i$. The quadratic term $\epsilon\epsilon^\mathrm{T}$ in $\mathbf{W}$ then dominates $U_i^\mathrm{T}\mathbf{W}U_i$. Therefore

$$\epsilon\epsilon^\mathrm{T} = \epsilon_i^2 U_i(\lambda)RR^\mathrm{T}U_i(\lambda)^\mathrm{T} = \epsilon_\mathrm{i}^2\sum_j(R_j^2)$$

and the first correction to s_i^2 in eq A1 is

$$U_i^\mathrm{T}\mathbf{W}U_i = \epsilon_i^2\sum_j(R_j^2)$$

When data are collected on a logarithmic time base, the sum over R_j^2, and therefore also the correction to s_i^2, grows as $(kt_\mathrm{f})^2$, where t_f is the last time point in the data set. We must also consider the second-order terms in eq A1, through which the linear term $\epsilon\mathbf{A}_0^\mathrm{T}$ in $\mathbf{W}$ also generates a correction to s_i^2. In the simplest case where $\mathbf{A}_0$ is a time-independent data set, i.e., $\mathbf{A}_0 = s_k^\mathrm{o}U_k(\lambda)V_k(t)^\mathrm{T}$ and all elements of V_k are identical

$$(U_i^\mathrm{T}\mathbf{W}U_k)^2/(s_i^{\mathrm{o}2} - s_k^{\mathrm{o}2}) \propto s_k^{\mathrm{o}2}\epsilon_i^2\left(\sum_j R_j\right)^2/(s_i^{\mathrm{o}2} - s_k^{\mathrm{o}2}) \approx -\epsilon_i^2\left(\sum_j R_j\right)^2$$

Again for a logarithmic time base, the sum over R_j grows in proportion to kt_f, so that this correction to s_i^2 also grows as $(kt_\mathrm{f})^2$. Thus s_i^2 grows as $(kt_\mathrm{f})^2$, and the new singular value s_i grows in proportion to kt_f and ϵ_i. Since the concentration of the new chemical species also grows in proportion to kt (at early times), the growth of a new singular value in Figure 4 mirrors the growth in the concentration of the new species. The amplitude of the new singular value is also proportional to ϵ_i, or the amplitude of the spectral change associated with the new species. This linear dependence of s_i on t_f is apparent in the logarithmic plot of Figure 4, where s_2/s_1 first rises above the noise background with nearly unit slope, since $\mathbf{A}_0$ is indeed time-independent. (The same general conclusions still apply when $\mathbf{A}_0$ is time-dependent, although the t_f dependence of s_i will not be linear.)

REFERENCES

1. Bushnell, G. W., Louie, G. V., and Brayer, G. D. (1990) *J. Mol. Biol. 214*, 585−595.
2. Jones, C. M., Henry, E. R., Hu, Y., Chan, C.-K., Luck, S. D., Bhuyan, A., Roder, H., Hofrichter, J., and Eaton, W. A. (1993) *Proc. Natl. Acad. Sci. U.S.A. 90*, 11860−11864.
3. Hagen, S. J., Hofrichter, J., Szabo, A., and Eaton, W. A. (1996) *Proc. Natl. Acad. Sci. U.S.A. 93*, 11615−11617.
4. Hagen, S. J., Hofrichter, J., and Eaton, W. A. (1997) *J. Phys. Chem. B 101*, 2352−2365.
5. Hagen, S. J., Carswell, C. W., and Sjolander, E. W. (2001) *J. Mol. Biol. 305*, 1161−1171.
6. Pascher, T., Chesick, J. P., Winkler, J. R., and Gray, H. B. (1996) *Science 271*, 1558−1560.
7. Telford, J. R., Tezcan, F. A., Gray, H. B., and Winkler, J. R. (1999) *Biochemistry 38*, 1944−1949.
8. Chen, E., Wood, M. J., Fink, A. L., and Kliger, D. S. (1998) *Biochemistry 37*, 5589−5598.
9. Chen, E., Wittung-Stafshede, P., and Kliger, D. S. (1999) *J. Am. Chem. Soc. 121*, 3811−3817.
10. Goldbeck, R. A., Thomas, Y. G., Chen, E., Esquerra, R. M., and Kliger, D. S. (1999) *Proc. Natl. Acad. Sci. U.S.A. 96*, 2782−2787.
11. Elove, G. A., Bhuyan, A. K., and Roder, H. (1994) *Biochemistry 33*, 6925−6935.
12. Sosnick, T. R., Mayne, L., Hiller, R., and Englander, S. W. (1994) *Nat. Struct. Biol. 1*, 149−156.
13. Colón, W., Wakem, L. P., Sherman, F., and Roder, H. (1997) *Biochemistry 36*, 12535−12541.
14. Ausubel, P. M., Brent, R., Kingston, R. E., Moore, D. D., Seidman, J. G., Smith, J. A., and Struhl, K. (1993) in *Current Protocols in Molecular Biology*, Greene Publishing Associates, Inc., and Wiley, New York.
15. Sambrook, J., Fritsch, E. F., and Maniatis, T. (1989) in *Molecular Cloning: A Laboratory Manual*, Cold Spring Harbor Laboratory, Cold Spring Harbor, NY.
16. Dolgikh, D. A., Latypov, R. F., Abdullaev, Z. Kh., Colón, W., Roder, H., and Kirpichnikov, M. P. (1998) *Bioorg. Chem. (Moscow) 24*, 756−759.
17. Pollock, W. B. R., Rosell, F. I., Twitchett, M. B., Dumont, M. E., and Mauk, A. G. (1998) *Biochemistry 37*, 6124−6131.
18. Babul, J., and Stellwagen, E. (1972) *Biochemistry 11*, 1195−1200.
19. Henry, E. R., and Hofrichter, J. (1992) *Methods Enzymol. 210*, 129−192.
20. Beechem, J. M. (1992) *Methods Enzymol. 210*, 37−53.
21. Arcovito, A., Gianni, S., Brunori, M., Travaglini Allocatelli, C., and Bellelli, A. (2001) *J. Biol. Chem. 276*, 41073−41078.
22. White, D. K., Cannon, J. B., and Traylor, T. G. (1979) *J. Am. Chem. Soc. 101*, 2443−2454.
23. Muthukrishnan, K., and Nall, B. T. (1991) *Biochemistry 30*, 4706−4710.
24. Grosberg, A. Y., and Khokhlov, A. R. (1994) *Statistical Physics of Macromolecules*, AIP Press, Woodbury, NY.
25. Camacho, C. J., and Thirumalai, D. (1995) *Proc. Natl. Acad. Sci. U.S.A. 92*, 1277−1281.
26. Thirumalai, D. (1999) *J. Phys. Chem. B 103*, 608−610.
27. Lapidus, L. J., Eaton, W. A., and Hofrichter, J. (2000) *Proc. Natl. Acad. Sci. U.S.A. 97*, 7220−7225.
28. Bieri, O., Wirz, J., Hellrun, B., Schutkowski, M., Drewello, M., and Kiefhaber, T. (1999) *Proc. Natl. Acad. Sci. U.S.A. 96*, 9597−9601.

BI011371A